J Mater Sci (2011) 46:3942–3951
DOI 10.1007/s10853-011-5319-9

Effective manipulation of the microstructure of zeolite film by hydrothermal pretreatment

Yi Liu · Yanshuo Li · Weishen Yang

Received: 18 October 2010 / Accepted: 22 January 2011 / Published online: 5 February 2011

Abstract Zeolite films with diverse microstructures were prepared from highly regular seed monolayers by accurate manipulation of various synthetic parameters during secondary growth. The effects of the hydrothermal pretreatment procedure, hydrothermal pretreatment temperature and duration, secondary growth temperature and duration of prepared zeolite films on final microstructures were investigated in detail. Based on these results, a mechanism was proposed to elucidate the effects of hydrothermal pretreatment on the secondary growth dynamics of the zeolite films: hydrothermal pretreatment could induce the separation of secondary nucleation and the subsequent growth process. Consequently, the disordered growth of zeolite films could be effectively avoided.

Introduction

Zeolites are crystalline materials with highly regular sub-nanometer-sized pore systems. Taking Mordenite Framework Inverted (MFI) zeolite [1] (symmetry: orthorhombic; space group: P_{nma}; unit cell constants: $a = 20.1$ Å, $b = 19.9$ Å, and $c = 13.4$ Å) as an example, the pore system consists of straight channels (pore size: 0.53 × 0.56 nm) interconnected by zigzag channels (0.51 × 0.55 nm) [2]. In addition to their traditional uses as catalysts, adsorbents and ionic exchangers [3], zeolites can also be fabricated into thin films and used as separation membranes [4–8], selective sensors [9, 10], low-*k* materials [11, 12], corrosion-resistant coatings [13], and optical materials [14, 15]. In the synthesis of high-quality zeolite films, the accurate manipulation and optimization of their microstructures, such as crystallographic preferred orientation (CPO), thickness, intergrowth and grain boundary structures, is critical. These microstructures may dramatically influence the performance of devices incorporating zeolite films.

Fine control of the CPO of zeolite films is especially critical [16]. Yan et al. synthesized highly *b*-oriented, i.e., (0 *k* 0) crystal planes arranged parallel to substrate-MFI films in situ on smooth stainless steel plates by accurately manipulating the synthetic conditions [17, 18]. In subsequent electrochemical testing, these films showed excellent molecular sieving properties as selective sensors [10]. Tsapatsis et al. fabricated twin-free and highly *b*-oriented MFI membranes by secondary growth of *b*-oriented MFI seed monolayers [4, 5]. Compared to randomly oriented membranes, the *b*-oriented membrane demonstrated dramatic improvements in both permeance and selectivity in the separation of *p*-/*o*-xylene vapors. Yoon et al. prepared highly *c*-oriented, fluorophore-containing LTL-type zeolite monolayers by inducing well-defined molecular linkages between LTL microcrystals and the substrates, and anisotropic photoluminescence was observed in the subsequent experiment [15].

Oriented zeolite films can be synthesized by methods including in situ growth, secondary growth, solid-state transformation [19], and laser ablation [20]. Compared with other approaches, secondary growth is better suited for the fabrication of oriented zeolite films, as film quality

Y. Liu · Y. Li · W. Yang (✉)
State Key Laboratory of Catalysis, Dalian Institute of Chemical Physics, Chinese Academy of Sciences, 457 Zhongshan Road, Dalian 116023, China
e-mail: yangws@dicp.ac.cn
URL: http://yanggroup.dicp.ac.cn/

Y. Liu
Graduate School of Chinese Academy of Sciences, Beijing 100049, China

is less affected by substrate conditions, and reproducibility is relatively high. Recently, new progress had been made in fabricating oriented zeolite films in a more elegant way. Lai et al. fabricated highly *c*-oriented $AlPO_4$-5 seed monolayers by manual assembly of uniform hexagonal seed plates and synthesized a preferentially *c*-oriented and continuous $AlPO_4$-5 film by optimizing secondary growth conditions [21]. Tsapatsis et al. fabricated a *c*-oriented $AlPO_4$-5 film from a sparsely deposited seed layer. Through hydrothermal pretreatment of the precursor solution, *c*-oriented growth of the seed layer became predominant in secondary growth [22]. An *a*-oriented ETS-10 film with columnar grain boundary microstructures was recently grown on an ITO glass substrate by secondary growth of a preferentially *a*-oriented ETS-10 seed multilayer [23]. We recently synthesized highly *a*- and *b*-oriented zeolite T membranes by microwave-assisted secondary growth of preferentially oriented seed layers. These membranes exhibited excellent ethanol/water pervaporation performance, with separation factors greater than 10,000 [24]. Jeong et al. established a new method for the synthesis of *b*-oriented MFI films with rare twin crystals [25]. Uniform, coffin-shaped MFI microcrystals were manually assembled into a *b*-oriented monolayer, on which a thin, passive Au/Pd layer was consequently sputtered. Then secondary growth was permitted, and in-plane growth of the seed layer was preserved. The undesirable twin growth was suppressed to a certain extent due to the presence of passive layer.

Secondary growth remains the most effective way to synthesize oriented MFI films due to its relatively high reproducibility and lower dependence on substrate conditions [26]. However, undesirable twin growth on the *b*-oriented MFI layer, in which MFI films evolve with (*k* 0 0) crystal planes arranged parallel to substrate (Fig. 1), often arises during secondary growth. Twin growth reduces the performance of the prepared zeolite films, and should be inhibited as much as possible [4]. The most effective way to fabricate highly *b*-oriented MFI films with minimal twin crystals is using template *trimer*-TPAOH instead of TPAOH during secondary growth. However, a more elegant and cost-effective method of preparing high-performance MFI films is required for future commercial applications.

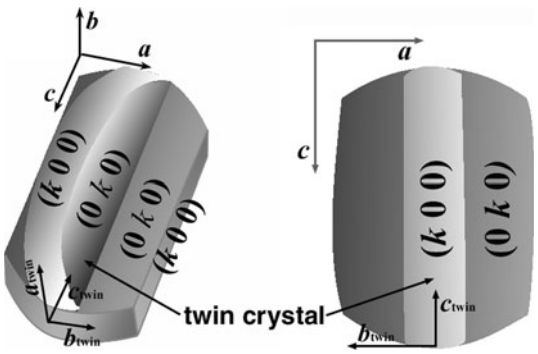

Fig. 1 Schematic illustration of the relevant crystal planes and directions on MFI twin crystal

In previous work, we presented a novel interface-aided seeding method to fabricate a compact and highly *b*-oriented MFI monolayer [27]. Recently, using this monolayer as the seed layer, we reported a new technique for the synthesis of highly *b*-oriented MFI films with minimal twin crystals [28]. Hydrothermal pretreatment of the precursor solution before secondary growth was the key step for the effective inhibition of twin growth on the *b*-oriented MFI seed layer. Tsapatsis and Karanikolos also succeeded in synthesizing highly *c*-oriented $AlPO_4$-5 films by thermal pretreatment of the precursor solution [22]. But further research was required to clarify the influence of various synthetic parameters on the final microstructures of the prepared MFI films. More importantly, the effects of hydrothermal treatment on the growth dynamics of MFI seed layers must be further elucidated. This paper presents a detailed study intended to produce a more comprehensive understanding of this process. Based on these results, we propose a mechanism to account for the effects of hydrothermal pretreatment on the growth modes of *b*-oriented MFI seed layers during secondary growth.

Experiment

Synthesis of MFI microcrystals

MFI (silicalite-1) microcrystals were synthesized with slight modification to the well-documented procedure [5]. For a typical synthesis, 7.6 g TPAOH (tetrapropylammonium hydroxide, 20 wt%, Aldrich) and 7.5 g TEOS (tetraethyl orthosilicate, 98%, Kermal) were mixed with 60.0 g DDI (distilled de-ionized) water. The mixture was further aged at room temperature for 24 h, and then transferred to a Teflon-lined vessel and placed in an oil bath and stirred. The temperature was maintained at 130 °C for 12 h, and the vessel was then removed and cooled to room temperature. The products were centrifuged at 6,000 rpm, washed three times with DDI water, and then air-dried at 50 °C in an oven overnight. The MFI microcrystals synthesized in this way were coffin-shaped, with an average size of 1.6 μm.

Substrate pretreatment

Before deposition of MFI seeds, a 2 cm × 2 cm glass substrate was washed with DDI water, immersed in a

piranha solution (H_2SO_4/H_2O_2 = 2/1 v/v), heated to 90 °C and maintained for 1 h to remove organic impurities. After this, the substrate was washed with copious DDI water and stored in pure ethanol.

b-Oriented MFI seed layer deposition

To prepare an alcohol-modified zeolite suspension, 0.02 g MFI microcrystals were mixed with 5 mL *sec*-butanol and 1 μL linoleic acid, and vigorously stirred in a cone-shaped bottle at room temperature for more than 6 days before use.

The self-assembly process was conducted at 25 °C with 60% RH. Initially, the pre-cleaned 2 cm × 2 cm glass plate was placed onto a horizontal plane. Then 0.8 mL of DDI water was injected onto this substrate. After formation of a uniform water layer, zeolite suspension was slowly and continuously injected onto the water layer using an automatic injector (TJ-1A, Baoding Longer Precision Pump Co., Ltd.) at the speed of 2 μL min^{-1} until a continuous MFI layer formed at the air–water interface. With controlled evaporation of the liquid layer, MFI microcrystals spontaneously self-assembled into a compact and highly *b*-oriented monolayer on the substrate. Finally, the templates plugged in the seed layer were removed by calcination at 550 °C with a ramp speed of 0.2 K/min.

Secondary growth

The molar composition of this synthetic solution was $5SiO_2$:1TPAOH:$1000H_2O$:20EtOH. With the sequential addition of TEOS (98%, Kermel) and TPAOH (20 wt%, Aldrich) into DDI water, the mixture was further aged at 25 °C for 4 h. Before secondary growth, this clear precursor solution was poured into an autoclave. This autoclave was then statically placed in a convective oven preheated to the desired temperature. After a predetermined time elapsed, it was removed and quenched to room temperature. Solid precipitates were then removed from the solution by centrifugation (12,000 rpm).

The seeded substrate was then vertically placed in this pre-heated solution, put into an autoclave and subject to secondary growth under given conditions. Then it was removed and quenched in a water bath. The MFI film was then washed, dried, and prepared for characterization.

The secondary growth procedure of MFI seed microcrystals in a powder form was similar to that of MFI layers, with slight modifications. In brief, 0.02 g of calcined MFI microcrystals and 20 mL of precursor solution were mixed together. After vigorous stirring for 1 h, they were poured into a vessel and subject to hydrothermal growth under given conditions.

XRD and SEM characterization condition

Morphologies of the MFI seed monolayer and the films were observed by scanning electron microscopy (Quanta 200 FEG, FEI Co., 30 kV). XRD patterns were recorded on a Rigaku D/MAX 2500/PC instrument using Cu Kα radiation (λ = 0.154 nm at 40 kV and 200 mA).

Results and discussion

Morphology of MFI building blocks

Prepared MFI microcrystals were subject to SEM characterization. As shown in Fig. 2a, most MFI microparticles synthesized in this way exhibited a coffin-shaped morphology with an average size of 1.6 μm. The XRD pattern (Fig. 2b) further confirmed that MFI was the only structure type present. Figure 2c provided a schematic illustration of their morphology. The largest facet corresponded to (0 *k* 0) crystal planes, while the neighboring crystal facet was associated with (*k* 0 0) crystal planes. These highly regular

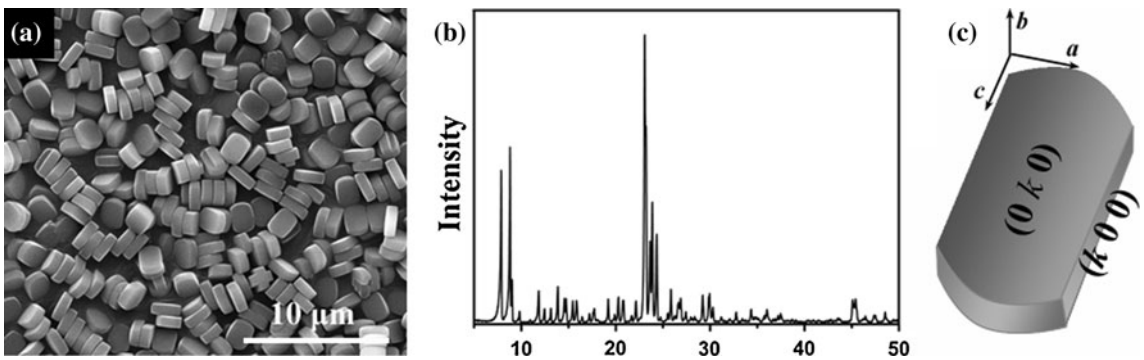

Fig. 2 **a** SEM image of prepared MFI microcrystals, and **b** XRD pattern of the MFI seeds, and **c** schematic illustration of the detailed morphological features of MFI microcrystals

microcrystals were used as microbuilding blocks in the subsequent self-assembly process.

Secondary growth with the precursor solution subject to hydrothermal pretreatment

Before secondary growth, the precursor solution had been hydrothermally pretreated at 150 °C for 2 h. At this point, systematic investigations were carried out to study the influence of the secondary growth temperature (at 130, 150, and 170 °C) and duration (for 1.5, 3, and 5 h) on the morphologies of prepared MFI films. Figure 3 showed that at a fixed temperature (e.g., 130 °C), with the extension of the reaction duration, the MFI seeds gradually grew larger (Fig. 3a) and began to merge with each other (Fig. 3b). Eventually, the intercrystalline space was fully filled by the secondary growth portion (Fig. 3c). But further prolonging the reaction duration induced undesired *a*-oriented growth, which gradually became more and more severe (typically Fig. 3k). Moreover, the higher the synthetic temperature, the shorter the synthetic time required to completely seal the gaps in the seed layer: 5 h at 130 °C, 3 h at 150 °C, and less than 3 h at 170 °C (Fig. 3c, f, i). So we concluded that high-quality MFI films could be synthesized by combining appropriate secondary growth temperature and duration.

XRD patterns (Fig. 4) further confirmed that twin growth of the seed layer was effectively inhibited by the accurate manipulation of synthetic conditions. These films were synthesized at 130, 150, and 170 °C, with identical

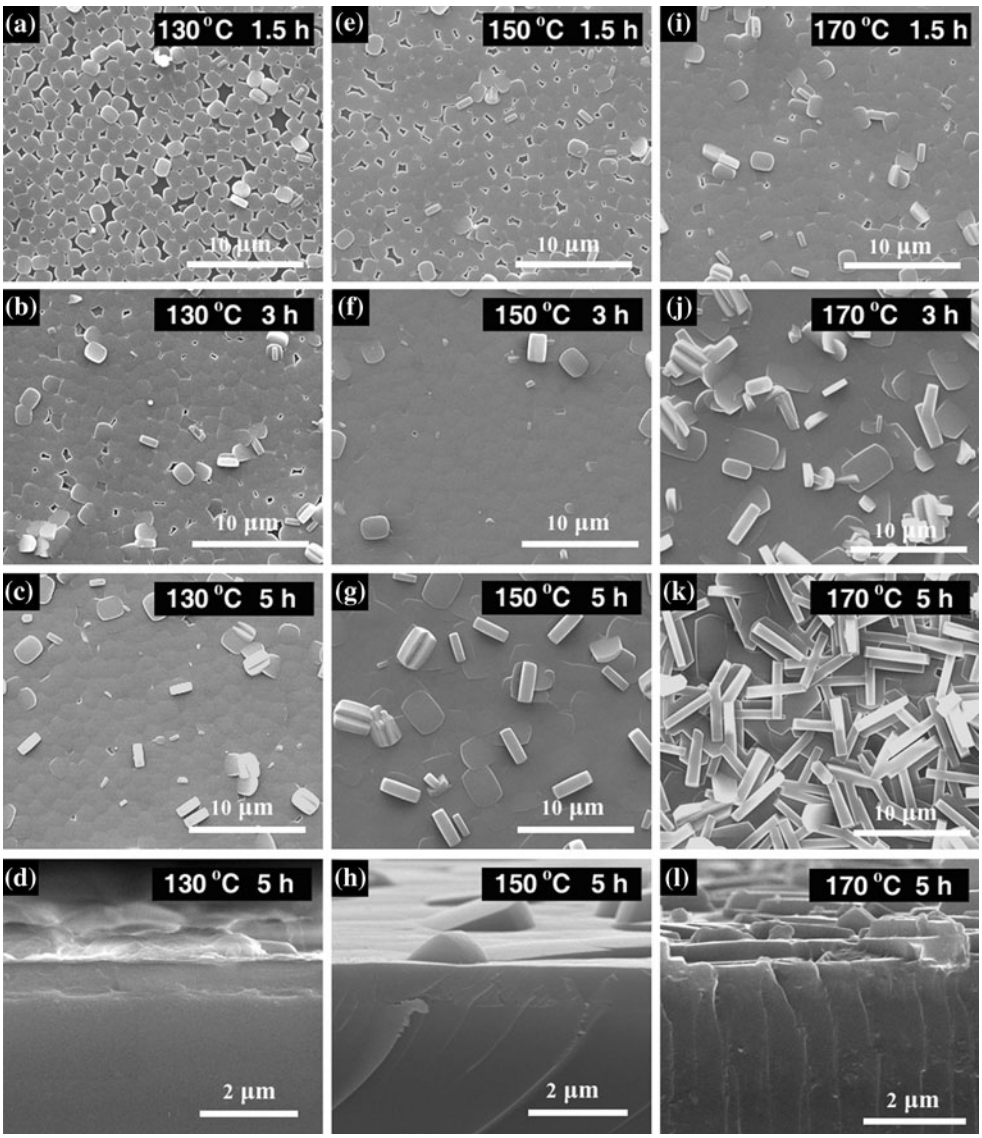

Fig. 3 SEM images of MFI films synthesized in secondary growth solutions subject to hydrothermal pretreatment at 150 °C for 2 h. The secondary growth was initiated at **a–d** 130 °C, **e–h** 150 °C, and **i–l** 170 °C for 1.5, 3, and 5 h, respectively

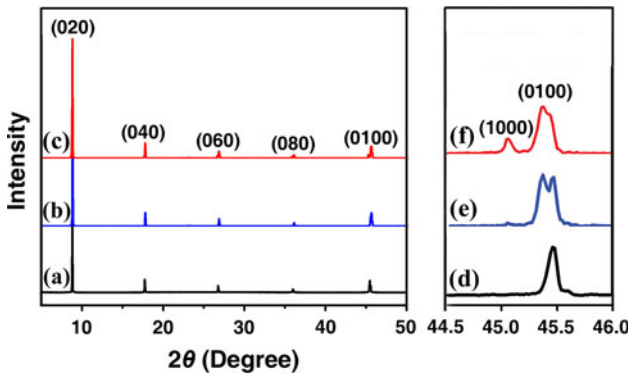

Fig. 4 XRD patterns of the MFI films synthesized in the secondary growth solution subject to hydrothermal pretreatment at 150 °C for 2 h. The secondary growth was maintained at (*a*) 130 °C, (*b*) 150 °C, and (*c*) 170 °C for 5 h with 2θ at 5°–50°; (*d*), (*e*), and (*f*) are enlarged images. *Note*: prepared MFI films were not calcined before XRD characterization

secondary growth periods of 5 h. As shown in Fig. 4, the (0 10 0) peaks of all these diffraction patterns split into two parts. In our previous work, the split sections of the (0 10 0) diffraction peak were identified as the secondary growth portion of the zeolite film and the original calcined seed layer, respectively. We noticed that increases in the synthesis temperature led to much higher intensity of secondary growth, implying acceleration of the *b*-oriented in-plane growth rate of the seed layer. The cross-sectional images also showed that the prepared MFI films synthesized at higher temperature were thicker, increasing from 0.7 to 1.3 μm (Fig. 3d, h, l), implying that the secondary growth portion gradually accounted for a larger proportion. Meanwhile, the (10 0 0) diffraction peak was substantially strengthened at 170 °C, illustrating that *a*-oriented twin growth was greater at a higher synthetic temperature.

Secondary growth with precursor solution not subject to hydrothermal pretreatment

If the precursor solution were not pretreated before secondary growth, twin growth (also known as the epitaxial growth along *a*-direct or (*k* 0 0) crystal faces) would arise before the complete sealing of the growing MFI seed layers, potentially leading to significantly decreased performance of the prepared films [4]. Here, systematic investigations were also conducted to elucidate the influence of the synthetic parameters on the final microstructures of the zeolite films (Fig. 5). At a fixed synthetic temperature (e.g., 130 °C), with the extension of the duration of secondary growth, these MFI seeds gradually grew larger (Fig. 5a), and began to merged with each other (Fig. 5b). Undesirable *a*-oriented epitaxial growth also arose simultaneously (Fig. 5b). The longer the reaction duration, the more severe the *a*-oriented growth (Fig. 5c). Similarly, when secondary growth duration was fixed (e.g., 3 h) and synthesis temperature was increased, undesirable twin growth also became more and more serious (Fig. 5b, f, j). Within the scope of our investigation, before the complete sealing of intercrystalline spaces between MFI seeds, the epitaxial growth of the MFI seed layer along the *b*-direction did play a dominant role, while the *a*-oriented twin growth was not obvious (Fig. 5a, e, i). However, once the gaps were sealed, substantial twin growth became inevitable (Fig. 5c, g, k). For instance, at 150 °C, the size of twin crystals dramatically increased from 0.7 μm after 1.5 h to 3 μm after 5 h. But twin crystals were rare when hydrothermal pretreatment was initiated under similar reaction conditions (Fig. 3g).

These films were also subject to XRD characterization. Figure 6 showed that when the secondary growth duration was fixed to 5 h, the intensity of the (10 0 0) diffraction peak very quickly strengthened with increases in the synthesis temperature. When secondary growth was initiated at 170 °C, the intensity of the (10 0 0) diffraction peak even overwhelmed the (0 10 0) peak. These results clearly illustrated that higher secondary growth temperature was more favorable for the twin growth of the seed layer if the synthetic time was fixed.

The influence of hydrothermal pretreatment parameters on microstructures of MFI films

After hydrothermal pretreatment, solids were precipitated from the solution. In contrast to results reported by Davis et al. [29], we found that MFI crystals evolved from the pre-formed amorphous phase.

It was necessary to systematically investigate the influence of hydrothermal pretreatment parameters on the microstructures of the prepared zeolite films. In our experiment, the hydrothermal pretreatment temperature was changed from 110 to 185 °C, and the preheating duration was fixed at 2 h. As shown in Fig. 7, twin growth of the *b*-oriented seed layer could be effectively inhibited at hydrothermal pretreatment temperatures between 130 and 170 °C (Figs. 7b, 3f, c). However, if the pretreatment temperature was 110 °C (Fig. 7a), extensive twin growth arose during secondary growth; in contrast, increasing the synthetic temperature to 185 °C led to incomplete intergrowth among the MFI seeds (Fig. 7d), probably due to the over-consumption of the nutrient during the hydrothermal pretreatment.

The effect of the duration of hydrothermal pretreatment was also investigated. The preheating temperature was fixed at 150 °C, while the hydrothermal pretreatment duration was changed from 0.5 to 12 h. As shown in Fig. 8, high-quality *b*-oriented MFI films were obtained at pretreatment durations from 1 to 5 h (Figs. 8b, 3f, c). If the

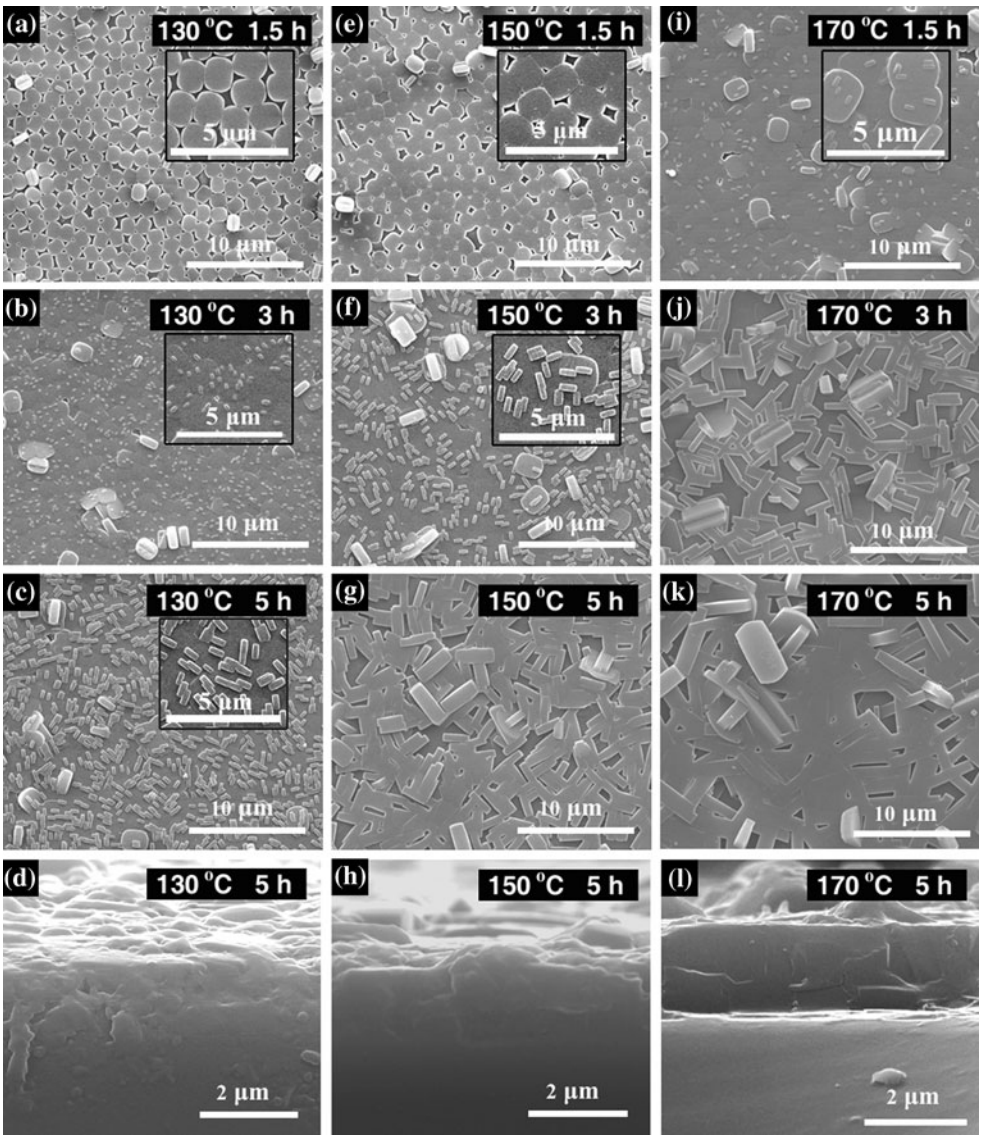

Fig. 5 SEM images of MFI films synthesized in secondary growth solutions not subjected to hydrothermal pretreatment. The secondary growth was initiated at **a–d** 130 °C, **e–h** 150 °C, and **i–l** 170 °C for 1.5, 3, and 5 h, respectively

preheat time was 0.5 h (Fig. 8a), twin growth was not effectively suppressed during secondary growth. At longer durations of hydrothermal pretreatment of the precursor solution (e.g., 12 h, see Fig. 8d), some bare space would remain uncovered by the MFI films after secondary growth, possibly due to insufficient nutrient supply.

In summary, we found that without hydrothermal treatment, undesirable twin growth of the *b*-oriented MFI seed layer spontaneously arose during secondary growth. This twin growth could not be easily eliminated by simple optimization of the synthetic conditions, but a continuous and highly *b*-oriented MFI film with minimal twin growth was easily produced by proper heat treatment of the precursor solution combined with appropriate secondary growth conditions. In the following section, we further discussed the effects of hydrothermal pretreatment on the growth dynamics of *b*-oriented MFI seed layers during secondary growth.

Growth mechanism of *b*-oriented MFI seed layers

As shown above, hydrothermal pretreatment exerted great influence on the final microstructures of prepared MFI films. To elucidate the growth mechanism of MFI seed layers during secondary growth, the synthesis process was investigated in detail at 130 °C. As shown in Fig. 9, if the precursor solution was not preheated before hydrothermal synthesis, then new MFI nuclei formed and grew on the *b*-oriented MFI seed layer at the initial stage of secondary growth (Fig. 9a). Subsequently, with the extension of the

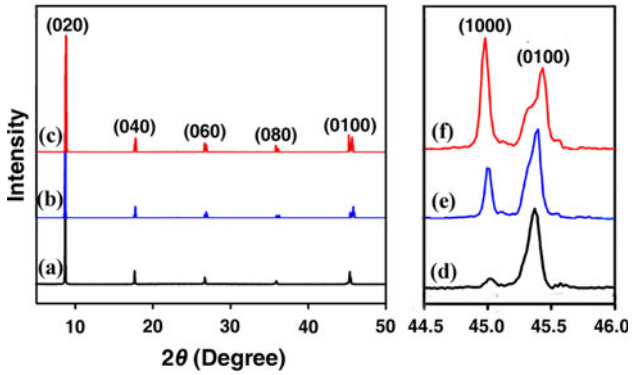

Fig. 6 XRD patterns of MFI films synthesized in secondary growth solutions not subjected to hydrothermal pretreatment. The secondary growth was maintained at (*a*) 130 °C, (*b*) 150 °C, and (*c*) 170 °C for 5 h with 2θ at 5°–50°; (*d*), (*e*), and (*f*) are enlarged images. *Note*: prepared MFI films were not calcined before XRD characterization

synthesis duration, these newly formed seeds gradually grew larger and larger, and began to merge with each other (Fig. 9b). Finally, the original *b*-oriented MFI seed layer was fully covered by the secondary growth portion (Fig. 5c). Simultaneously, undesirable twin growth arose and became more and more severe (Fig. 9c), probably due to the high nutrient concentration in the solution.

In contrast, when the precursor solution was hydrothermally pretreated before the secondary growth, a continuous and uniform epitaxial layer gradually formed on the surface of the *b*-oriented MFI seed layer (Fig. 9d, e). At the prolonged synthesis durations, these original MFI seeds gradually grew larger and began to merge with each other (Fig. 9f). As a result, the gaps among these MFI seeds were fully filled (Fig. 3c).

In summary, when the precursor solution was directly used in secondary hydrothermal synthesis, the original seed layer served as an intermediate layer to facilitate nucleation and subsequent growth of the newly formed zeolite crystals on the substrate. However, once the hydrothermal treatment was carried out, only uniform epitaxial growth of the original *b*-oriented seed microcrystals was initiated during the secondary growth. The change in growth modes could be interpreted as follows. First, through the hydrothermal pretreatment, MFI nuclei formed in the precursor solution. As a result, during secondary growth, new heterogeneous nucleation on the *b*-oriented seed layer, which was one cause of twin growth [4], was effectively avoided, and only the epitaxial growth of the original MFI seed layer was maintained during the secondary growth. Second, as the nutrient was largely

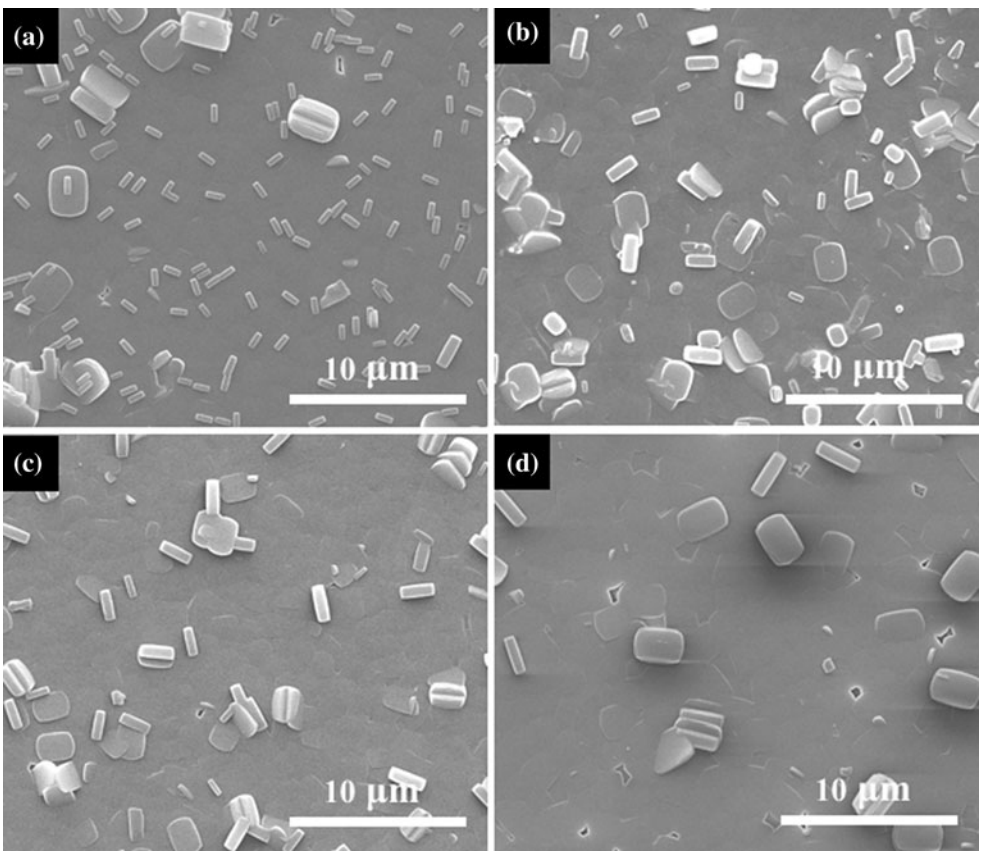

Fig. 7 SEM images of MFI films synthesized in secondary growth solutions subjected to hydrothermal pretreatment at (**a**) 110 °C, (**b**) 130 °C, (**c**) 170 °C, and (**d**) 185 °C with the duration of 2 h. The secondary growth was initiated at 150 °C for 3 h

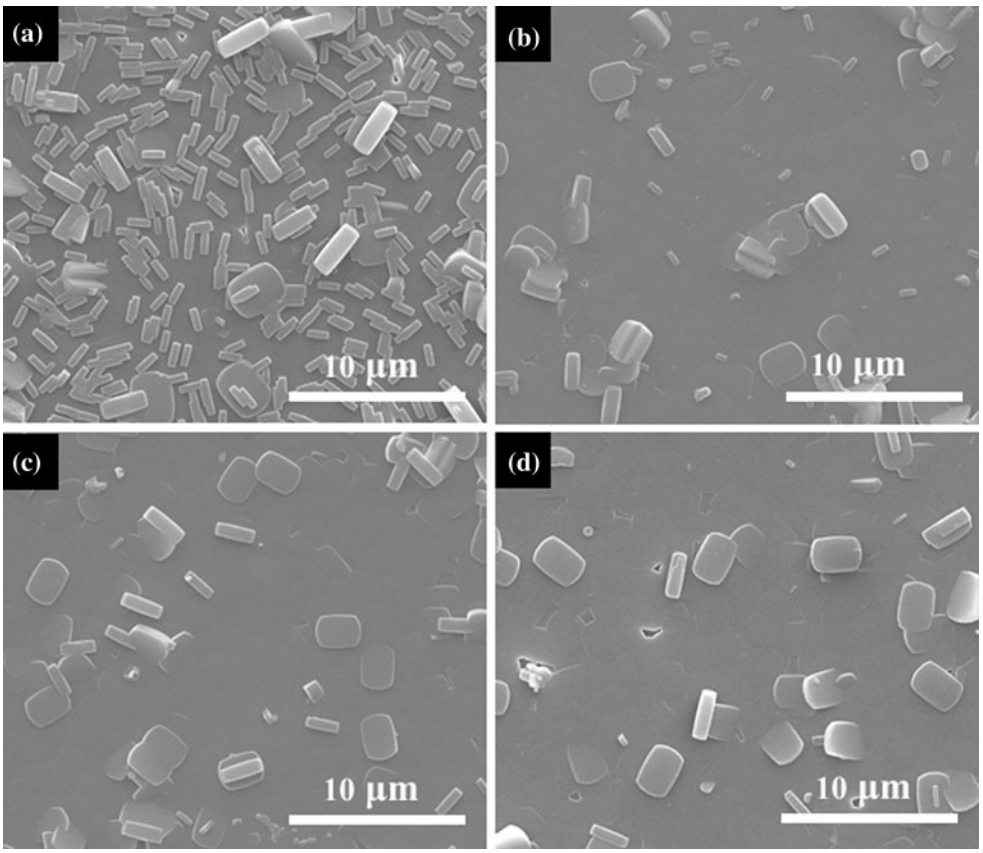

Fig. 8 SEM images of MFI films synthesized in secondary growth solutions subjected to hydrothermal pretreatment at 150 °C with durations of (**a**) 0.5 h, (**b**) 1 h, (**c**) 5 h, and (**d**) 12 h. The secondary growth was initiated at 150 °C for 3 h

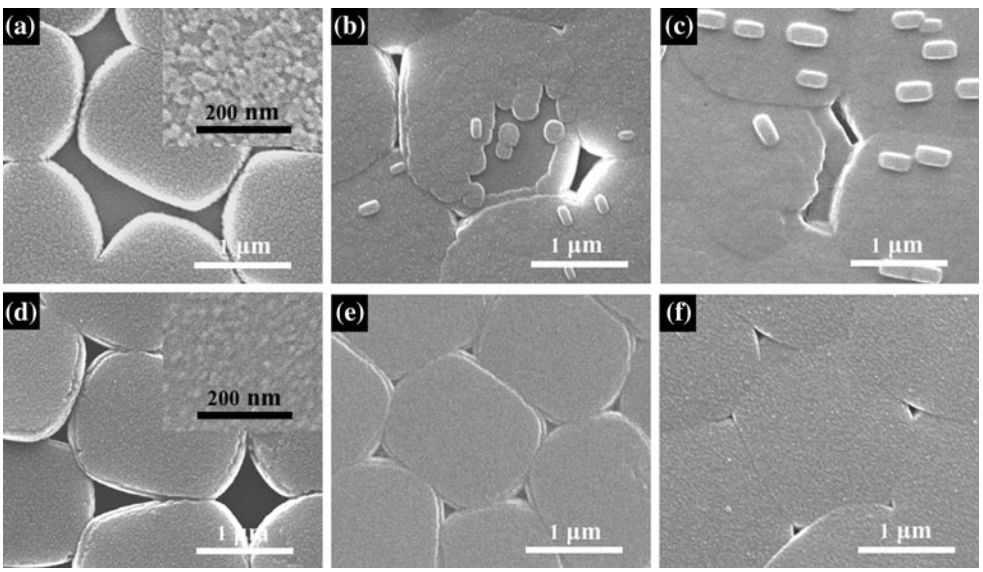

Fig. 9 SEM images of MFI films synthesized in secondary growth solutions not subjected to hydrothermal pretreatment. The secondary growth was initiated at 130 °C for (**a**) 1 h, (**b**) 2 h, and (**c**) 3 h, respectively; the MFI films were synthesized in secondary growth solutions subjected to hydrothermal pretreatment at 150 °C for 2 h. The secondary growth was initiated at 130 °C for (**d**) 1 h, (**e**) 2 h, and (**f**) 3 h, respectively

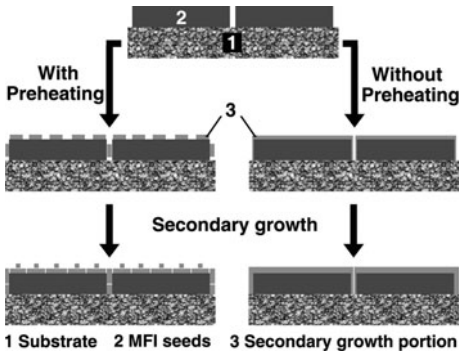

Fig. 10 Illustration of the growth mechanism of *b*-oriented MFI monolayers during secondary growth with the precursor solution subjected to and/or not subject to hydrothermal pretreatment

consumed in preheating, substantial twin growth of the seed layer was sustained in this process. Recently, in the hydrothermal pretreatment-induced synthesis of highly *c*-oriented $AlPO_4$-5 film by Tsapatsis et al., the microstructure transition from random orientation to *c*-preferred orientation was also ascribed to the nutrient dilution effect induced by pre-crystallization. Moreover, they deduced that the in-plane secondary growth proceeded through the oriented intergrowth of the original $AlPO_4$-5 seeds [22]. These results confirmed the rationality of our model, but further verification was still necessary. Two different growth modes of the *b*-oriented MFI seed layers during secondary growth were also illustrated in Fig. 10.

The growth dynamics of MFI seed microcrystals in powder form during secondary growth was also investigated (Fig. 11). Without hydrothermal pretreatment, heterogeneous nuclei ($\sim$50 nm in size) also nucleated on MFI seed microcrystals (Fig. 11a). They gradually grew larger, merged with each other, and fully covered the surface of the original MFI microparticles (Fig. 11b). Finally, the *a*-oriented epitaxial growth appeared (white arrows, as shown in Fig. 11c). In contrast, when subject to hydrothermal treatment, no evidence of heterogeneous nucleation and twin growth was observed during the whole process (Fig. 11d–f). Throughout the experiment, similar microstructure evolution processes were observed during the secondary growth of MFI microcrystals in both layer and powder forms. These results also shed light on the design and fabrication of MFI microcrystals with more sophisticated microstructures, which may be beneficial to optimizing their performance for various practical applications.

Conclusions

Highly *b*-oriented MFI films with minimal twin crystals were synthesized by secondary growth of *b*-oriented MFI seed layers. By hydrothermal pretreatment of the precursor solution, *b*-oriented in-plane growth was maintained while undesirable twin growth was substantially suppressed during secondary growth. The influence of various synthetic parameters on the final microstructures of prepared MFI films was investigated in detail. It was found that high-quality MFI films with desired microstructures could

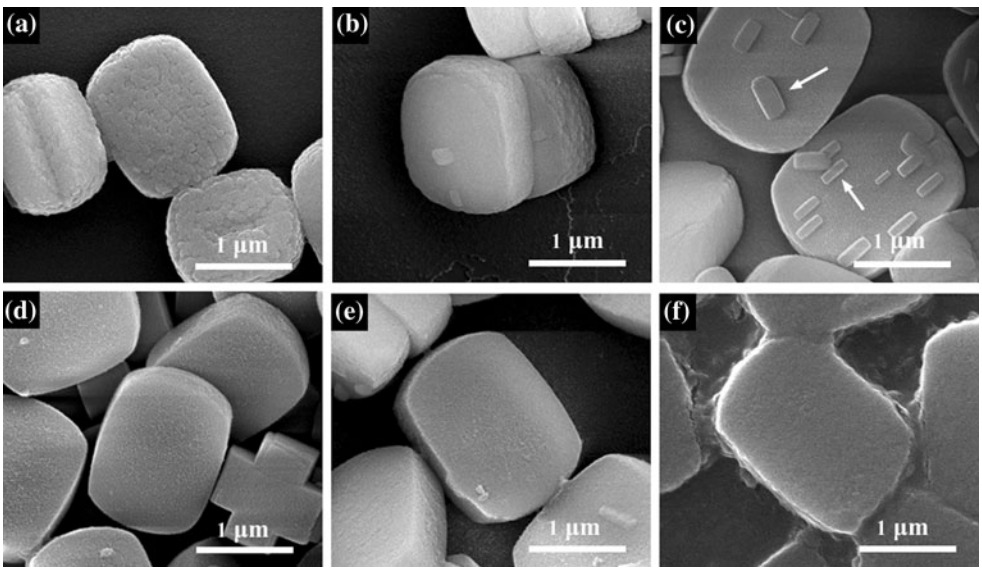

Fig. 11 SEM images of MFI microcrystals after growth in secondary growth solutions not subjected to hydrothermal pretreatment. The secondary growth was initiated at 130 °C for (**a**) 1 h, (**b**) 2 h, and (**c**) 3 h, respectively; and MFI microcrystals after growth in secondary growth solutions subjected to hydrothermal pretreatment at 150 °C for 2 h. The secondary growth was initiated at 130 °C for (**d**) 1 h, (**e**) 2 h, and (**f**) 3 h, respectively

be synthesized under lenient conditions, which could simplify the manufacturing process and prove beneficial in scalable applications. Based on these results, we proposed a mechanism for interpreting the effects of hydrothermal pretreatment on the growth dynamics of *b*-oriented MFI seed layers: for precursors not subjected to hydrothermal pretreatment, secondary nucleation and subsequent twin growth on the original MFI seed layers were inevitable; however, for hydrothermally pretreated precursors, the nucleation process could be avoided, and only uniform epitaxial growth occurred during secondary growth.

Acknowledgements This work was supported by the National Science Fund for Distinguished Young Scholars (20725313), the DICP Independent Research Project (No. R200807), and the Ministry of Science and Technology of China (Grant No. 2003CB615802).

References

1. Xia HA, Sun KQ, Feng ZC, Li C J Phys Chem C. doi: 10.1021/jp1094917
2. Mentzen BF (2007) J Phys Chem C 111:18932
3. Davis ME (2002) Nature 417:813
4. Lai ZP, Bonilla G, Diaz I, Nery JG, Sujaoti K, Amat MA, Kokkoli E, Terasaki O, Thompson RW, Tsapatsis M, Vlachos DG (2003) Science 300:456
5. Lai ZP, Tsapatsis M, Nicolich JP (2004) Adv Funct Mater 14:716
6. Choi J, Jeong H, Snyder MA, Stoeger JA, Masel RI, Tsapatsis M (2009) Science 325:590
7. Zhu GQ, Li YS, Chen HL, Liu J, Yang WS (2008) J Mater Sci 43:3279. doi:10.1007/s10853-008-2524-2
8. Carreon MA, Li S, Falconer JL, Noble RD (2008) J Am Chem Soc 130:5412
9. Li S, Wang X, Beving D, Chen ZW, Yan YS (2004) J Am Chem Soc 126:4122
10. Gora L, Kuhn J, Baimpos T, Nikolakis V, Kapteijn F, Serwicka EM (2009) Analyst 134:2118
11. Cai R, Sun MW, Chen ZW, Munoz R, O'Neill C, Beving DE, Yan YS (2008) Angew Chem Int Ed 47:525
12. Liu Y, Sun MW, Lew CM, Wang JL, Yan YS (2008) Adv Funct Mater 18:1732
13. Cai R, Yan YS (2008) Corrosion 64:271
14. Shu G, Liu JM, Chiang AST, Thompson RW (2006) Adv Mater 18:185
15. Lee JS, Lim H, Ha K, Cheong H, Yoon KB (2006) Angew Chem Int Ed 45:5288
16. Snyder MA, Tsapatsis M (2007) Angew Chem Int Ed 46:7560
17. Wang ZB, Yan YS (2001) Microporous Mesoporous Mater 48:229
18. Wang ZB, Yan YS (2001) Chem Mater 13:1101
19. Chaikittisilp W, Davis ME, Okubo T (2007) Chem Mater 19:4120
20. Balkus KJ, Muñoz T, Gimon-Kinsel ME (1998) Chem Mater 10:464
21. Hu EP, Huang YLW, Yan Q, Liu DP, Lai ZP (2009) Microporous Mesoporous Mater 126:81
22. Veziri CM, Palomino M, Karanikolos GN, Corma A, Kanellopoulos NK, Tsapatsis M (2010) Chem Mater 22:1492
23. Galioğlu S, Ismail MN, Warzywoda J, Sacco A, Akata B (2010) Microporous Mesoporous Mater 131:401
24. Zhou H, Li YS, Zhu GQ, Liu J, Yang WS (2009) Sep Purif Technol 65:164
25. Lee I, Buday JL, Jeong HK (2009) Microporous Mesoporous Mater 122:288
26. McLeary EE, Jansen JC, Kapteijn F (2006) Microporous Mesoporous Mater 90:198
27. Liu Y, Li YS, Yang WS (2009) Chem Commun 45:1520
28. Liu Y, Li YS, Yang WS (2010) J Am Chem Soc 132:1768
29. Davis TM, Drews TO, Ramanan H, He C, Dong J, Schnablegger H, Katsoulakis MA, Kokkoli E, Mccormick AV, Penn RL, Tsapatsis M (2006) Nat Mater 5:400